

## Mechanical model of an earthquake fault

J. M. Carlson and J. S. Langer

*Institute for Theoretical Physics, University of California, Santa Barbara, California 93106*

(Received 21 July 1989)

We examine the dynamic behavior of a simple mechanical model of an earthquake fault. This model, introduced originally by Burridge and Knopoff [Bull. Seismol. Soc. Am. 57, 341 (1967)], consists of an elastically coupled chain of masses in contact with a moving rough surface. Our version of the model retains the full Newtonian dynamics with inertial effects and contains no externally imposed stochasticity or spatial inhomogeneity. The only nonlinear feature is a velocity-weakening stick-slip friction force between the masses and the moving surface. This system is being driven persistently toward a slipping instability and, therefore, exhibits noisy sequences of earthquakelike events. We observe these events in numerical simulations and are able to predict many of their features analytically. Their size distributions are found numerically to be consistent with the Gutenberg-Richter law. Some aspects of the size distributions can be understood by scaling arguments.

### I. INTRODUCTION

Recently, Bak, Tang, and Weisenfeld<sup>1</sup> have called attention to the fact that many systems in nature operate persistently at or near thresholds of instability, and that such systems might be expected to exhibit anomalously large, "critical" fluctuations. The prototypical example is a pile of sand onto which new grains are added very slowly. Once a sandpile achieves steady state, it is expected theoretically to exhibit avalanches with a wide range of sizes as its slope fluctuates in the neighborhood of a critical angle of repose.<sup>2</sup> An example of more immediate interest, especially for those of us who live in California, is an earthquake fault. The surface at which two moving tectonic plates come into contact with one another is persistently being driven toward a slipping instability; and the slipping events, i.e., earthquakes, are observed to occur with a wide range of magnitudes.<sup>3,4</sup>

In this investigation, we examine the behavior of a very simple mechanical model of an earthquake fault. The class of models that we consider was introduced over twenty years ago in the seismological literature by Burridge and Knopoff.<sup>5,6</sup> Unlike the cellular automata studied by Bak and his co-workers,<sup>1,3</sup> the Burridge-Knopoff model is a purely deterministic dynamical system that consists of blocks and springs and obeys Newton's laws of motion. It is driven persistently toward a slipping instability induced by a nonlinear, velocity-weakening friction law similar to the stick-slip coupling between the bow and string of a violin.<sup>7</sup>

Our main conclusion<sup>8</sup> is that, without the addition of any intrinsic spatial irregularities or external stochastic forces, this model is capable of generating noisy sequences of slipping events whose size distribution is similar in important respects to what is seen in seismological measurements. Specifically, the majority of the events that we observe—although not always the largest events—are distributed in size according to the

Gutenberg-Richter law;<sup>4</sup> that is, the logarithm of the frequency of events decreases linearly with their magnitude. We observe such distributions in numerical simulations and are able to describe many of their features by scaling arguments. We also are able to predict properties of the individual events by analytic methods. Although the model is more nearly a caricature than an accurate picture of an earthquake fault, its features are sufficiently realistic that we can begin to relate its various kinds of dynamic behavior to physical characteristics such as stiffness of the rock, the velocity dependence of the friction force, and the speed at which the plates are being driven across each other. The results of this study also provide some guidance about how to make more realistic, predictive models of seismic phenomena.

There are interesting and possibly useful similarities between the threshold criticality that we find in the Burridge-Knopoff model and the behavior of other systems of current scientific interest. For example, the sandpile analogy has been proposed as a model for flux flow in type-II superconductors.<sup>9</sup> The model also has elements in common with theories of pinning and depinning of charge-density waves in solids.<sup>10</sup> Another situation that looks at least superficially similar is a moving line of contact between a wetting layer and its substrate, for example, the upper edge of a drop of water as it slips intermittently down a window pane.<sup>11</sup>

The scheme of this paper is as follows. In Sec. II, we describe our version of the Burridge-Knopoff model and define the several dimensionless groups of parameters that govern its behavior. Sections III and IV are devoted to analytic discussions of various features of this model—the instability of spatially uniform motions and three qualitatively different kinds of nonuniform slipping events. Our numerical solutions are presented in Sec. V, which contains both pictures of the slipping events and a statistical analysis of their frequencies of occurrence. In Sec. VI, we point out that these size distributions seem to

describe scale-invariant critical fluctuations with a nonuniversal “anomalous dimension,” and we show how this result may be used to predict the frequency of great events which lie outside the critical region. Several fundamental questions regarding the interpretation and significance of our results are addressed in Sec. VII. The paper concludes in Sec. VIII with a brief summary of our results.

## II. BASIC FEATURES OF THE MODEL

Our version of the Burridge-Knopoff model<sup>5</sup> is illustrated in Fig. 1. It differs from the original primarily in that our system is taken to be completely uniform with no spatial variations of any of its parameters and no externally determined stochastic elements. It consists of a chain of blocks of mass  $m$  coupled to each other by harmonic springs of strength  $k_c$  and attached to a fixed surface, shown above the blocks in the figure, by leaf springs or torsion elements of strength  $k_p$ . The blocks are in contact with a rough substrate which is moving at speed  $v$  to the left as shown. Equivalently, the substrate may be fixed and the blocks pulled to the right by the upper surface acting through the “pulling springs”  $k_p$ . In a qualitative sense, the blocks may be thought of as the points of contact between two plates moving at relative speed  $v$  along a lateral fault. The spring constants  $k_c$  and  $k_p$  describe the linear elastic response of the contact region to compression and shear, respectively. The equations of motion for the model remain the same if the blocks are being displaced transversely, that is, in a direction perpendicular to the chain. In this case, the model would look roughly like the line of contact between two plates moving across each other at a subduction zone.

The crux of the model is the velocity-dependent force of friction  $F$  between the blocks and the surface, shown schematically by the solid curve in Fig. 2. Throughout most of this analysis, we shall assume an idealized stick-slip law, as shown here, with a static friction that can take on all values between  $-F_0$  and  $+F_0$  at precisely zero velocity, and with a sliding friction that decreases

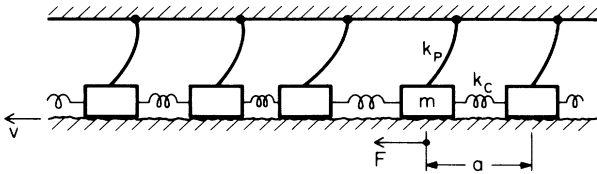


FIG. 1. Block and spring system for the Burridge-Knopoff model. In our analysis, we assume that the system is spatially homogeneous, composed of equal masses  $m$ , each connected to its nearest neighbors by springs of strength  $k_c$ , and to a stationary surface with springs of strength  $k_p$ . Each mass is subject to the friction force  $F(\dot{X})$ , which depends only on the velocity of the block. The equilibrium spacing is  $a$ , which does not enter directly into the equation of motion (2.1).

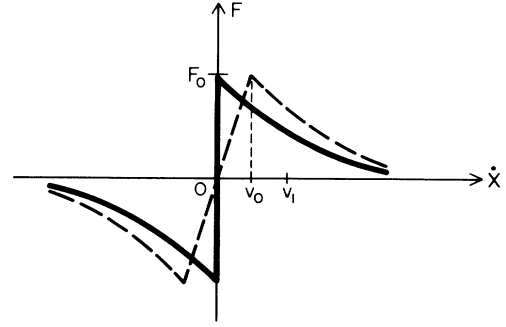


FIG. 2. The slip-stick friction law. The function  $F(\dot{X})$  ranges between  $\pm F_0$  at zero velocity and decreases monotonically to zero as  $|\dot{X}|$  becomes large. Our numerical calculations are based on the solid curve, for which  $F(\dot{X})$  decreases to half of its maximum value at the characteristic speed  $v_1$ . The dashed curve describes slow, stable creep for a small range of speeds  $|\dot{X}| < v_0$ , and has the same velocity-weakening behavior as the solid curve for speeds of order  $v_1$ . Because the dashed curve is single valued for all  $\dot{X}$ , the continuum limit Eq. (2.8) is well defined for this choice of the friction law, and the velocity  $v_0$  determines a small-scale cutoff for slipping events as described in Eq. (7.2).

monotonically with increasing slipping speed. This friction law introduces the only nonlinearity in the system and is responsible for the instability that generates chaotic behavior. In this regard, we differ from much of the recent work in this field in that we do not assume a state-dependent friction law or otherwise introduce explicit memory effects.<sup>12-17</sup> On the other hand, we do retain inertial terms.

The equations of motion for this model are

$$m\ddot{X}_j = k_c(X_{j+1} - 2X_j + X_{j-1}) - k_p X_j - F(v + \dot{X}_j), \quad (2.1)$$

where dots indicate derivatives with respect to time  $t$  and the  $X_j$  are the displacements of blocks  $j$  measured from their initial equilibrium positions. For the friction law  $F$  we assume a function of the form

$$F(\dot{X}) = F_0 \phi(\dot{X}/v_1), \quad (2.2)$$

where  $\phi$  vanishes at large values of its argument and is normalized so that  $\phi(0) = -\phi'(0) = 1$ , and  $v_1$  is some speed that characterizes the velocity dependence of  $F$ .

We begin the analysis of (2.1) by rewriting it in a scaled form that gives us some insight concerning the roles played by the various lengths and times that occur in this system. A natural choice for a timelike variable is

$$\tau = \omega_p t, \quad \omega_p^2 = k_p/m. \quad (2.3)$$

The quantity  $2\pi/\omega_p$  is the period of oscillation of a single block attached to a pulling spring in the absence of sliding friction. The maximum displacement of such a block before slipping is  $D_0 = F_0/k_p$ , which is a natural unit in which to measure  $X$

$$X_j = D_0 U_j = (F_0/k_p) U_j. \quad (2.4)$$

In these units, (2.1) becomes

$$\ddot{U}_j = l^2(U_{j+1} - 2U_j + U_{j-1}) - U_j - \phi(2\alpha v + 2\alpha \dot{U}_j), \quad (2.5)$$

where

$$l^2 = k_c/k_p, \quad v = v/(\omega_p D_0), \quad 2\alpha = \omega_p D_0/v_1, \quad (2.6)$$

and dots now denote differentiation with respect to  $\tau$ . The three dimensionless groups of parameters defined in (2.6) are the fundamental quantities that govern the behavior of this system.

The dimensionless pulling speed  $v$  is the ratio of the slipping time  $\omega_p^{-1}$  to the loading time  $D_0/v$ , where the latter is the time that it takes for a pulling spring to be stretched enough to overcome the static friction. For very large events on real earthquake faults, slipping times may be of order seconds and loading times of order tens or hundreds of years; thus realistic values of  $v$  are less than  $10^{-8}$ . The parameter  $\alpha$  is the ratio of the largest characteristic slipping speed  $\omega_p D_0$  to the speed  $v_1$  at which friction is appreciably reduced. We expect the model to exhibit larger undamped motions for larger values of  $\alpha$ .

Note that there is no natural length scale for measuring position along the fault; the equilibrium spacing between the blocks, denoted by  $a$  in Fig. 1, so far appears nowhere in these equations. The fact that the scaling of distances along the fault is arbitrary and completely independent of the units in which we measure the displacements  $X_j$  is important for understanding certain properties of this model. Although it is not mathematically necessary to introduce the length  $a$  explicitly, there are several practical reasons for doing so. First, assigning units to distance along the fault is useful for dimensional analysis. Second, it is convenient to be able to think of the continuum limit of this model as one in which  $a \rightarrow 0$ , as opposed to a limit in which the spacing remains fixed and the functions  $U$  are constrained to be arbitrarily slowly varying. Finally, we shall see that  $a$  has a physical role to play as a short-wavelength cutoff.

Accordingly, we introduce variables with dimensions of length

$$s = ja, \quad \xi = la = a(k_c/k_p)^{1/2}, \quad (2.7)$$

and—provisionally—take the limit  $a \rightarrow 0$  in order to write (2.5) in the form

$$\ddot{U} = \xi^2 \frac{\partial^2 U}{\partial s^2} - U - \phi(2\alpha v + 2\alpha \dot{U}). \quad (2.8)$$

Equation (2.8) is not actually a well-defined partial differential equation. There would be no difficulty were we to introduce an arbitrarily narrow stable-creep region at small velocities as shown by the dashed line in the figure; we shall discuss the effects of such a modification in Sec. VII. For the idealized law, however, the multiple-valued character of  $\phi$  at  $\dot{U}=0$  causes the system to undergo discontinuous stick-slip events all the way down to the one-block level; in other words, the numerical discretization of (2.8) that takes it back to (2.5) can

never be performed at so small a length scale that the stick-slip events will look spatially smooth. Nevertheless, (2.8) is a useful representation of the underlying finite-difference equation (2.5), and we frequently shall refer to the two equations interchangeably. We see from (2.8) that the length  $\xi$  is a stiffness or equivalently, because  $\tau$  is dimensionless, a sound speed. If  $\xi$  is to remain finite in the continuum limit, then  $l$ , the number of blocks in the length  $\xi$ , must diverge like  $a^{-1}$ . Working back through the various parameters that we have introduced, we find that  $m$ ,  $k_p$ , and  $F_0$  vanish linearly with  $a$  in this limit, and that  $k_c$  is proportional to  $a^{-1}$ .

### III. SOME SPECIAL SOLUTIONS

A trivial solution of (2.8) is

$$U = -\phi(2\alpha v) = \text{const}, \quad (3.1)$$

where the blocks are moving uniformly at the pulling speed relative to the rough surface. Because of the form we have chosen for the friction law, this solution is unstable against small perturbations of all wavelengths. To see this, write

$$U(s, \tau) = -\phi(2\alpha v) + u_1 \exp(iqs + \Omega\tau) \quad (3.2)$$

and linearize (2.8) in  $u_1$ . The amplification rate  $\Omega$  is found to be

$$\Omega(q) = \bar{\alpha} \pm (\bar{\alpha}^2 - 1 - \xi^2 q^2)^{1/2}, \quad (3.3)$$

which remains positive for all  $q$ . [ $\bar{\alpha} = -\alpha\phi'(2\alpha v) \cong \alpha$  for small  $v$ .] Because  $\text{Re}\Omega$  remains finite for all  $q$ , this instability is not the kind that causes divergences at finite times; deformations of arbitrarily short wavelength do not grow arbitrarily rapidly. On the other hand, any small irregularity in the positions of the blocks, no matter how long or short its wavelength, is amplified while the system is slipping in this manner.

A second spatially uniform solution of (2.8) is one in which  $U(\tau)$  undergoes periodic motion satisfying

$$\ddot{U} = -U - \phi(2\alpha v + 2\alpha \dot{U}). \quad (3.4)$$

A numerical solution of this equation is shown in Fig. 3, where we have plotted the displacement  $U$  and the velocity  $\dot{U}$  as functions of  $\tau$  for the case  $v=0.1$ ,  $\alpha=2.5$ . The system alternately sticks (until  $U$  has reached its limiting value  $-1$  where the force exerted by each pulling spring equals the maximum static friction) and then slips (until the pulling springs are sufficiently compressed to stop the motion) in unison, as if it were a single block. If  $\alpha$  is large, then  $\phi$  is small throughout most of each slipping event, and the solution of (3.4) for a slip that starts at  $\tau=0$  is  $U \cong -\cos(\tau)$ . Remember that the units of  $\tau$  have been chosen so that the slipping time  $\tau_S$  for this event is of order  $\pi$ . Because the total displacement in this limiting case is  $\delta U \cong 2$ , the system takes a time of order  $\tau_L = 2/v$ —the loading time in these units—to return to its slipping point  $U = -1$ .

This uniform stick-slip motion is also unstable. A linear stability analysis (not shown here in detail) indicates that, as the system passes through the region of

slipping speeds for which  $\phi'$  is negative, irregularities in the positions of the blocks are amplified by essentially the same mechanism that was described in the first paragraph of this section. This instability is illustrated in Figs. 4(a) and 4(b), which are three-dimensional represen-

tations of, respectively, the velocities  $\dot{U}_j$  and the strains, i.e., the differences  $U_{j+1} - U_j$ , as functions of  $\tau$ . We have started the system with all blocks stuck and with an almost imperceptibly weak, uneven departure from exactly uniform spacing. All blocks slip at approximately the same time, as they would in an exactly uniform configuration, but the irregularities are amplified strongly during the slipping event and the system is left in a highly irregular state once it comes to rest again.

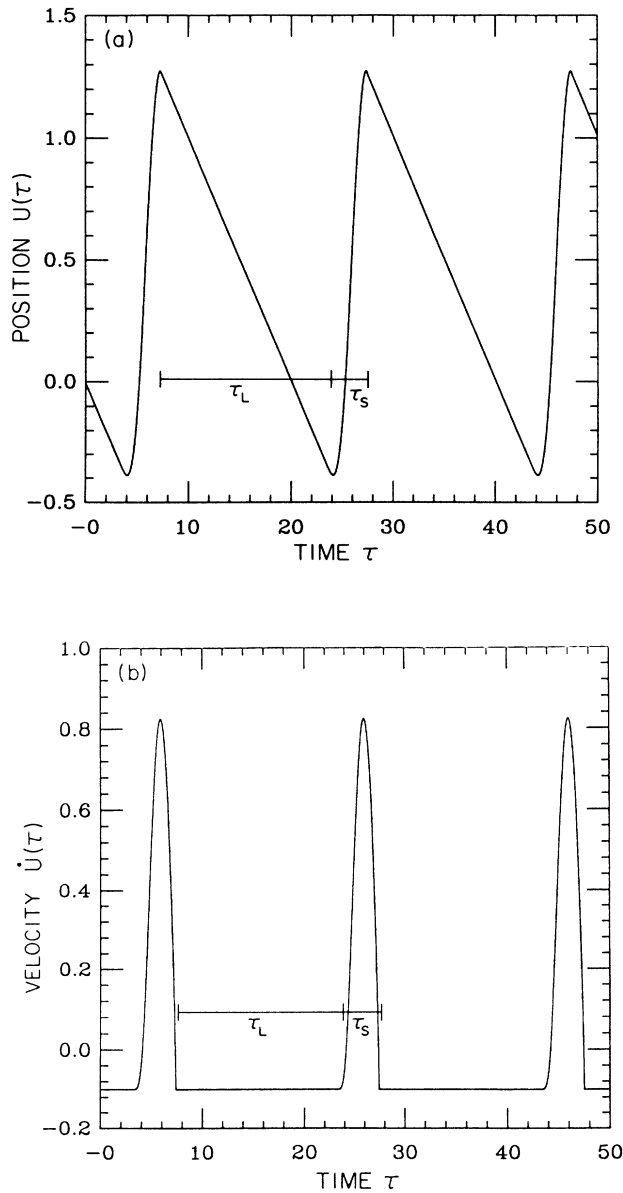


FIG. 3. Periodic solutions. When the initial conditions are spatially uniform, the system exhibits periodic stick-slip motion that is identical to the stable solution for a single block. In this solution, the blocks remain stuck for a time of order  $\tau_L = 2/\nu$  until they reach the threshold static friction, and then they slip for a time of order  $\tau_S \approx \pi$ . (a) and (b) illustrate, respectively, the dimensionless displacement  $U(\tau)$  and the velocity  $\dot{U}(\tau)$  for the case  $\alpha=2.5$ ,  $l=10$ , and  $\nu=0.1$ . Similar solutions may be obtained for propagating kinks as discussed in the text.

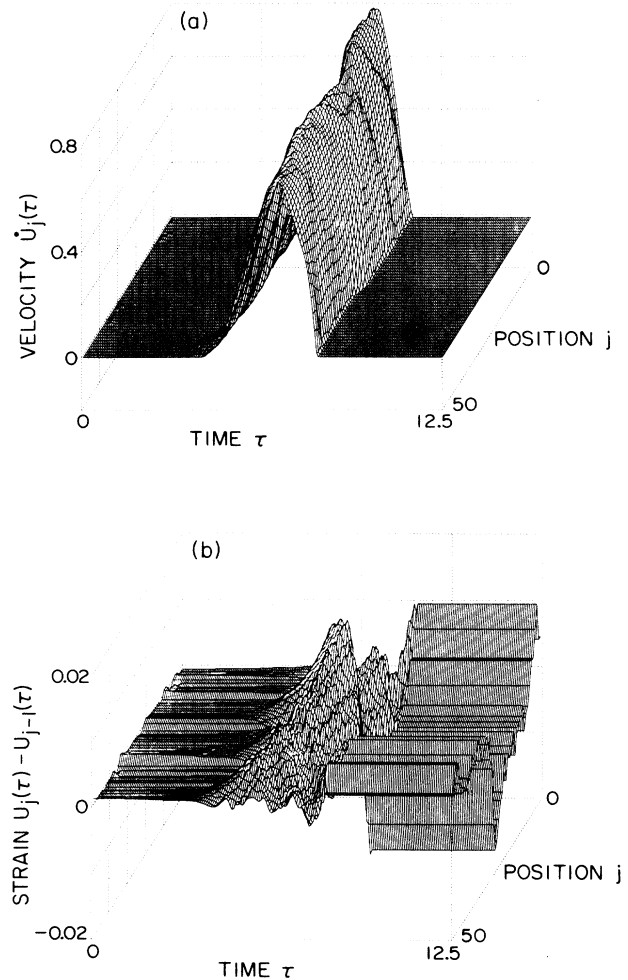


FIG. 4. Instability of uniform motion. We began this simulation with a small spatial inhomogeneity in the displacements. (a) illustrates the velocities  $\dot{U}_j(\tau)$ . As in Fig. 3 for uniform initial conditions, here we see that the most prominent feature is a large slipping event involving the whole system. In this case, however, the motion is somewhat irregular. The irregularity is more evident in (b), which shows the strains  $U_j(\tau) - U_{j-1}(\tau)$ . Here we see more clearly how the initial inhomogeneity is amplified during a great event. Afterwards, the system is left in a highly irregular configuration which gives rise to a sequence of smaller events before the next great event takes place. These results were obtained for  $\alpha=2.5$ ,  $l=10$ , and  $\nu=0.01$ .

Equation (2.8) also admits periodic solutions in the form of propagating kinks. If we write

$$U(s, \tau) = U(\tau \pm s / \beta), \quad (3.5)$$

then  $U$  satisfies

$$(1 - \xi^2 / \beta^2) \ddot{U} = -U - \phi(2\alpha v + 2\alpha \dot{U}), \quad (3.6)$$

which is almost the same as (3.4) except for the reduced "mass" on the left-hand side. These kinks must propagate at speeds  $\beta$  which are greater than the sound speed  $\xi$  in order that this mass remain non-negative. As functions of  $\tau$ , they look much like the uniform modes shown in Fig. 3 except that, as  $\beta$  approaches  $\xi$ , the slipping time decreases toward zero. In general, these propagating modes must be just as unstable as the uniform ones. As we shall see, kink propagation does appear in the larger events that occur in open systems, and a vestige of the system-wide, periodic solutions seems to coexist with chaotic behavior.

#### IV. EVENTS OF VARIOUS SIZES

Most of the slipping events that occur in numerical simulations of this model are not uniform or propagating motions of the system as a whole but, rather, involve smaller, connected groups of blocks. These events fall into three distinct categories that we shall describe, respectively, as "microscopic," "localized," and "delocalized." In order to understand what is seen in the simulations, it is useful first to look at events in each of these categories from an analytic point of view.

The microscopic events, by definition, involve only one or a few blocks. To describe them, we must use the discrete version of the equations of motion (2.5) rather than the continuum limit (2.8) in which such events are invisible. Consider a connected group of  $n$  blocks whose internal spacings are sufficiently uniform that the group slips as a whole between blocks on either side which remain stuck. Such a slipping event occurs when the group has fallen far enough behind its neighbors that the combined forces exerted by the  $n$  pulling springs and the two external coupling springs are equal to the maximum force of static friction. For example, the middle block in Fig. 1 may be in such a situation.

Let the position of the center of mass of this group  $U_{c.m.}$  be expressed in the form

$$U_{c.m.} = \frac{1}{n} \sum_{j=j_1+1}^{j_1+n} U_j = -v\tau + W_n. \quad (4.1)$$

Note that we have shifted to a frame of reference in which  $\dot{W}_n = 0$  when the blocks are stuck. The equation of motion for  $W_n$  is

$$\ddot{W}_n = -\Omega_n^2 W_n + 1 - \phi(2\alpha \dot{W}_n) + v\tau, \quad (4.2)$$

where

$$\Omega_n^2 = 1 + \frac{2l^2}{n}, \quad (4.3)$$

and we have chosen the origin of the time axis so that the

system will start slipping with  $W = \dot{W} = 0$  at  $\tau = 0$ . The form of these equations can be understood by noting that the pulling and frictional forces act equally on all the slipping blocks but, for any  $n$ , only the two coupling springs which connect the slipping blocks to the rest of the system have any effect on the center of mass. Thus, in (4.3), the relative effect of the coupling springs decreases as  $n$  becomes large.

For small  $n$ , we expect that the speed  $\dot{W}_n$  is small enough that  $2\alpha \dot{W}_n \ll 1$ . Then we can linearize  $\phi$  in (4.2) and write

$$\ddot{W}_n - 2\alpha \dot{W}_n + \Omega_n^2 W_n \cong v\tau. \quad (4.4)$$

The solution of this equation is

$$W_n(\tau) = \frac{v \exp(\alpha\tau)}{2\Omega_n^4 i \Gamma_n} [\Omega_n^2 \exp(i\Gamma_n \tau) - \Omega_n^2 \exp(-i\Gamma_n \tau)] + \frac{2\alpha v}{\Omega_n^4} + \frac{v\tau}{\Omega_n^2}, \quad (4.5)$$

where

$$\Omega_{\pm} = \alpha \pm i\Gamma_n, \quad \Gamma_n = (\Omega_n^2 - \alpha^2)^{1/2}. \quad (4.6)$$

Because  $l^2$  is generally a large number,  $\Gamma_n$  is real for sufficiently small  $n$  (or for any  $n$  if  $\alpha < 1$ ).

For small  $n$ , where  $\Omega_n \gg \alpha$ , the solution (4.5) becomes

$$W_n(\tau) \cong \frac{v}{\Omega_n^2} \left[ \tau - \frac{\sin(\Omega_n \tau)}{\Omega_n} \right]. \quad (4.7)$$

The group of blocks comes to rest after a time interval  $\delta\tau = 2\pi/\Omega_n$ , having moved forward a distance

$$\delta W_n = \frac{2\pi v}{\Omega_n^3} \cong 2\pi v \left[ \frac{n}{2l^2} \right]^{3/2}. \quad (4.8)$$

In this limit, the slipping condition is immediately satisfied at the moment the blocks come to rest and thus the motion repeats itself continuously. Note, however, that the average speed

$$\frac{\delta W_n}{\delta\tau} = \frac{v}{\Omega_n^2} \cong \frac{nv}{2l^2} \quad (4.9)$$

is much less than  $v$  for small  $n$ . Thus, although a group of blocks undergoing a sequence of these small periodic events is catching up with its immediate neighbors, it is falling further and further behind the average displacement of the system as a whole. In fact, this average speed vanishes in the continuum limit in which  $la$  and  $na$  remain fixed while  $a \rightarrow 0$ .

In a more accurate solution, which retains the effects of a nonzero  $\alpha$ , the group of blocks moves further forward than is indicated in (4.7) and sticks briefly between slipping events. We shall see that these periodic sequences of small events, usually involving only one or two blocks, are prominent features of our numerical simulations. As  $n$  increases,  $\Gamma_n$  decreases. Thus the larger slipping events last for longer times, the blocks undergo larger displacements, and the sticking time between events increases. Quite quickly, however, the approximations leading to

(4.4) fail, primarily because our assumption that the slipping blocks are uniformly spaced is unrealistic for any but very small values of  $n$ . What we have done, in effect, is to assume that the strain, and thus the energy stored in the coupling springs, is strongly localized at the ends of the slipping region. There is no reason for this to happen for large  $n$ .

To develop an analytic picture of larger events—those which we call localized or delocalized, and which contribute appreciably to the average forward motion of the system—we must go to the continuum limit, i.e., Eq. (2.8). In this limit, the condition that the blocks along some section of the chain be just on the verge of slipping is

$$\xi^2 \frac{d^2 U}{ds^2} - U = 1. \quad (4.10)$$

That is, the sum of the coupling and pulling forces just balances the maximum static friction continuously across the whole slipping zone. The general form of (4.10) implies that the strain  $dU/ds$  can be concentrated at most within regions of size  $\xi$  at the zone's boundaries. Specifically, the solutions  $U_\epsilon$  of (4.10) can be written

$$U_\epsilon(s) = -1 + \epsilon \cosh(s/\xi), \quad (4.11)$$

where we have arbitrarily chosen the zone to be centered at  $s=0$ , and have used the symbol  $\epsilon$  to denote the distance of closest approach between  $U_\epsilon(s)$  and the displacement  $U = -1$  at which the blocks must slip under the influence of the pulling springs alone.

Having identified a region in which a slipping event is about to occur, we now can ask what that event might look like. As long as we stay within the zone where (4.10) is satisfied, and as long as we never encounter negative slipping speeds, we can write  $U(s, \tau) = U_\epsilon(s) + u(s, \tau)$  and solve

$$\ddot{u} - \xi^2 \frac{\partial^2 u}{\partial s^2} + u = 1 - \phi(2\alpha v + 2\alpha \dot{u}) \cong 2\alpha \dot{u}. \quad (4.12)$$

In writing the second, approximate version of (4.12), we assume that the velocity  $\dot{u}$  is much bigger than the pulling speed  $v$ , but that  $\alpha \dot{u} \ll 1$  so that the motion does not probe the nonlinear portion of  $\phi$ . No other approximations are involved. The fact that neither  $\epsilon$  or the position of the slipping zone along the  $s$  axis (i.e.,  $s=0$ ) appear in (4.12) is an exact consequence of the fact that the only nonlinearity of (2.8) is contained in the velocity-dependent function  $\phi$ .

Suppose, now, that the slipping motion is triggered by a small pulse at some position, say  $s_0$ —presumably a slipping event on a scale appreciably smaller than the one we are considering. More generally, the motion may be triggered by a number of nearly simultaneous small pulses. Within our linear approximation, however, such a motion would be simply a linear superposition of the motions generated by the single pulses. For simplicity, we describe this event by the initial conditions

$$u(s, 0) = 0, \quad \dot{u}(s, 0) = w_0 \delta(s - s_0), \quad (4.13)$$

where  $w_0$  is proportional to the slipping speed during the

triggering event. More precisely, if the triggering event is the slipping of a single block, then, according to (4.7),

$$w_0 = \frac{va}{2l^2}, \quad (4.14)$$

the extra factor  $a$  being the width of the pulse. The subsequent motion is

$$u(s, \tau) = w_0 \int \frac{dq}{2\pi} \left[ \frac{\sin(\Gamma_q \tau)}{\Gamma_q} \right] \exp[iq(s - s_0) + \alpha \tau], \quad (4.15)$$

where  $q$  is a wave number and

$$\Gamma_q = (\xi^2 q^2 + 1 - \alpha^2)^{1/2}. \quad (4.16)$$

If we assume that the dominant contribution to the Fourier integral in (4.15) comes from wave numbers such that  $q\xi \gg \alpha$ , that is, that the pulse remains narrow compared to  $\xi/\alpha$ , then we find

$$\dot{u}(s, \tau) \approx \frac{1}{2} w_0 e^{\alpha \tau} [\delta(s - s_0 - \xi \tau) + \delta(s - s_0 + \xi \tau)]. \quad (4.17)$$

Here, two exponentially growing velocity pulses are propagating at the sound speed  $\xi$  in opposite directions away from the source point  $s_0$ .

If the slipping zone is not too large, the pulses must stop at the edges; they do not grow large enough to cause the blocks outside the zone to become unstuck and, thus remain localized. In fact, it seems unlikely that one would see well-resolved pulses in any but very large slipping zones. Because of the frictional instability, small propagating pulses—or superpositions of such pulses—must be very noisy.

On the other hand, in a very large zone where  $\epsilon$  is so small that  $U$  is close to its limiting value  $-1$  across a large part of the system, a pulse may become delocalized. It may grow enough that it dislodges blocks outside the initial slipping zone, and eventually may become so large that the linear approximation fails in (4.12). In this case, the pulse ceases to be amplified ( $\phi$  vanishes) and should look much like one of the propagating solutions of (3.6), perhaps with  $\beta \cong \xi$  and, accordingly, a sharp front that looks like a shock wave. We see both kinds of events—localized and delocalized—in the numerical simulations to be described in Sec. V. We shall present an explicit mathematical criterion for localization in Sec. VI, and this criterion will play an important role in our analysis of the numerical results.

One feature of this model that has not been given proper emphasis so far in this section is the amplification of spatial irregularities while blocks slip. Our assumption in analyzing both the small discrete events and the larger continuous ones has been that the system is locally smooth enough for an event of the appropriate size to occur. The initial state of the slipping zone, of course, is never ideally smooth, and we know from Sec. III that residual irregularities are amplified during the slipping process by the frictional instability. In fact, the exponential growth of the pulses in (4.17) is a manifestation of this same instability.

We thus are led to the following qualitative picture of

how chaotic behavior is generated in this model. An event of extent, say,  $\Delta s$  amplifies irregularities on scales smaller than  $\Delta s$ , and these irregularities subsequently produce smaller events. At the same time, because the blocks that are slipping in the zone  $\Delta s$  are catching up with their neighbors on the average, the event is smoothing the system on scales larger than  $\Delta s$  and, accordingly, is preparing it for larger events. In this way, the events of widely differing sizes that we have described in the preceding paragraphs are generated irregularly and persistently by the deterministic motion of this dynamical system. To learn more about this complex behavior, we turn next to numerical methods.

## V. NUMERICAL SOLUTIONS

We have solved Eq. (2.5) numerically for various choices of the parameters  $\alpha$ ,  $\nu$ , and  $l$ , with system sizes  $L = Na$  up to  $N=400$  blocks, and with a friction function of the form

$$\phi(y) = \frac{1}{1+|y|} \text{sgn}(y). \quad (5.1)$$

All results described here are for the case of free boundary conditions—the chain simply stops at its ends.

[We did try periodic boundary conditions in a few early tests with small systems ( $N=50$ ). In those cases, the

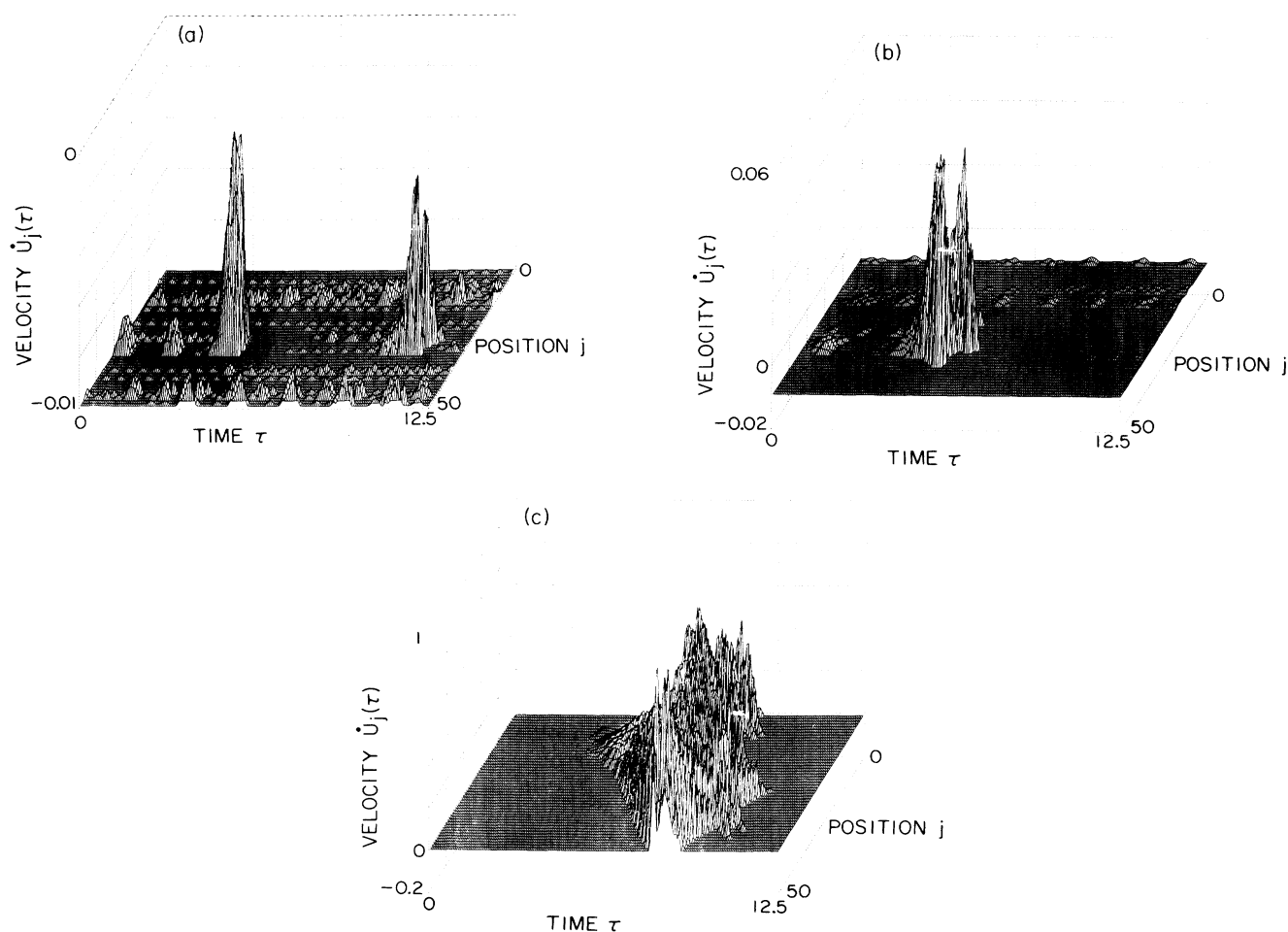


FIG. 5. Chaotic solutions. When the system has evolved from irregular initial conditions to a statistically steady state, we observe a wide range of events, shown here for  $\alpha=2.5$ ,  $l=10$ , and  $\nu=0.01$ . (a) illustrates the smallest slipping events. Periodic one- and two-block events are quite prominent, as well as two successive eight-block events. Note that the maximum velocity attained during the events shown here is less than the pulling speed  $\nu$  ( $\dot{U} < 0$ ); hence these events act mainly to smooth the system on small scales rather than to release appreciable amounts of strain. (b) illustrates an intermediately large localized event. Here the maximum velocity is much greater than  $\nu$ ; hence some strain is released locally. (c) illustrates a delocalized great event. Note that the event is triggered by a small slip in the interior of the system and propagates to the boundaries at the sound speed, as described in the text. The maximum velocity during this event is approximately the same as that of the uniform event shown in Fig. 3(b), but the motion in this case is highly irregular.

motion eventually settled down into smooth, periodic propagating modes of the form (3.5). This may have been a finite-size effect.]

Generally, we started the system in a fully stuck configuration with a small spatial inhomogeneity and allowed it to run for ten or more loading periods  $2/\nu$  before accumulating data. After the system reached what appeared to be a statistically steady state, we observed a wide range of events, some of which are illustrated in Figs. 5(a)–5(c) in the form of graphs of the velocities  $\dot{U}_j$  as functions of positions  $j$  and time  $\tau$ . The parameters used in computing these figures were  $\nu=0.01$ ,  $l=10$ ,  $\alpha=2.5$ , and  $N=50$ .

Figure 5(a) shows the system during a relatively quiet period. Note that the vertical scale is greatly expanded and that all events have maximum speeds that are less than the pulling speed  $\nu$  ( $\dot{U} < 0$ ). Most noticeable in the figure are two successive events involving the same group of eight blocks. Periodic, one-block, microscopic events of the kind described in Eq. (4.7) are much in evidence, as are a smaller number of two- and three-block events which are less regular and less persistently repetitive.

In Fig. 5(b), we show the system during a time interval in which a moderately large localized event occurred. The maximum speed now is appreciably larger than  $\nu$  and, in comparison, the one- and two-block events are hardly visible. On the other hand, the slipping speed achieved in this event is much less than unity, which, in our units, is the maximum velocity ( $\omega_p D_0$ ) of a great event like that shown in Fig. 3. Note the intrinsic irregularity of this event.

Figure 5(c) shows a delocalized great earthquake of the kind that occurs roughly once a loading period  $2/\nu$  for this choice of system parameters. This particular event is reasonably well described by (4.17). It is triggered by a small event in the interior of the system and the resulting disturbance grows as it propagates at the sound speed in both directions toward the edges. In this case the slipping speeds do approach unity. The event finally dies out as the moving pulses are reflected from the boundaries. Again, note the amplification of irregularities.

We have generated a large amount of numerical data of the kind illustrated here, and have analyzed it in terms similar to those used in the seismological literature. In particular, the statistical analysis of Gutenberg and Richter relates the frequency of seismic events to the Richter magnitude, the latter being a measure of the amplitude of the motion expressed on a (base ten) logarithmic scale. The analogous relationship for our version of the Burridge-Knopoff model is as follows.

Define the “moment”  $M$  of an event to be

$$M = \sum_j \delta U_j, \quad (5.2)$$

where the sum is over all blocks which are displaced during the event, and  $\delta U_j$  is the displacement of the  $j$ th block. The corresponding “magnitude” is  $\mu = \ln M$ . Let  $\mathcal{R}(\mu)d\mu$  be the frequency of events, per unit length of the fault, whose magnitudes are between  $\mu$  and  $\mu+d\mu$ . According to Gutenberg and Richter (who, by necessity, averaged over events observed throughout much of the

world, not just on one fault), this function has the form

$$\mathcal{R}(\mu) \cong \frac{A}{M^b} = A e^{-b\mu}, \quad (5.3)$$

where  $A$  is a constant (independent of  $M$ ), and  $b \cong 1$ . To the best of our knowledge, there has not yet been a first-principles, theoretical explanation of the  $b \cong 1$  law, nor has there been much understanding about how to compute the constant  $A$ .

Figures 6(a)–6(e) are graphs of  $\ln \mathcal{R}(\mu)$  obtained from our simulations with various values of the parameters  $\alpha$ ,  $l = \xi/a$ ,  $\nu$ , and  $N = L/a$ . The events in each case fall identifiably into the three categories described previously.

First, at the small- $\mu$  ends of the distributions, there are large numbers of microscopic events whose magnitudes, in accord with (4.8), are of order

$$\mu_n = \ln(na\delta W_n) = \ln \left[ 2\pi n a \nu \left( \frac{n}{2l^2} \right)^{3/2} \right]. \quad (5.4)$$

The quantity  $\mu_1$  (with  $a=1$ ) is marked explicitly in each graph and corresponds accurately to the position of the first peak in each distribution. Subsidiary peaks near  $\mu_2$ ,  $\mu_3$ , etc. are visible, but are increasingly broadened because larger groups of blocks can slip with larger variations of their internal configurations. Such variations are not accounted for in (5.4). As seen in Fig. 6(e), for example, these subsidiary peaks are more pronounced for larger values of  $\alpha$ , i.e., weaker sliding friction. They also are shifted toward larger  $\mu$  because (4.8) underestimates the displacements that would be obtained from (4.5) for large values of  $a$ .

Next, at the centers of these graphs, there are broad groups of moderately large events—we shall see that they are the localized events—whose distributions are consistent with the form (5.3). That is, the functions  $\ln \mathcal{R}(\mu)$  have linear regions with slopes  $-b$ . Moreover, for  $\alpha \geq 2.5$ , the exponent  $b$  is indistinguishable from unity, in agreement with the Gutenberg-Richter law. For reasons that will become apparent, we shall refer to the part of the distribution in which (5.3) is valid as the “scaling region,” and shall denote the function  $\mathcal{R}$  in this region by  $\mathcal{R}_S$ .

Finally, at the large- $\mu$  ends of the distributions, there are groups of events which are too frequent to be consistent with the scaling function (5.3). These are delocalized great events of the kind illustrated in Fig. 5(b). Their magnitudes may be, at most, of order  $\mu_L = \ln(2L)$  because the largest possible earthquake is one which displaces the entire fault a distance  $\delta U = 2$  and, therefore, has a moment  $2L$ . We can see from the figures that  $\mu_L$  is, in fact, an upper bound for  $\mu$ . In what follows, we shall denote the corresponding part of the distribution function by  $\mathcal{R}_G(\mu)$ . This feature seems always to be present, but, as seen in Fig. 6(d), is weaker for small  $\alpha$ . As seen in Fig. 6(c), the distribution  $\mathcal{R}_G$  becomes broader for larger values of  $L/\xi$ .

In addition to the results shown in Figs. 5 and 6, we have obtained data from simulations with a variety of other values of  $\alpha$ ,  $\nu$ , and  $L$ . The dependence on  $\alpha$  is particularly interesting. As  $\alpha$  decreases, slipping friction be-

comes less effective and, as a result, the motions become slower and the displacements smaller in each event. In Fig. 6(d), where  $\alpha=1$ , we see that the scaling distribution has become noticeably flatter— $b$  is considerably less than unity—so that the more extensive localized events have become relatively more frequent. For  $\alpha < 1$ , we have

found that these extended localized events tend to run into each other in a way that makes the definition of an isolated “event” required by (5.2) essentially meaningless. Note that the condition  $\alpha < 1$  implies that all of the modes in (4.16), no matter how small the wave number  $q$ , have oscillatory components; thus  $\alpha=1$  may be a limiting

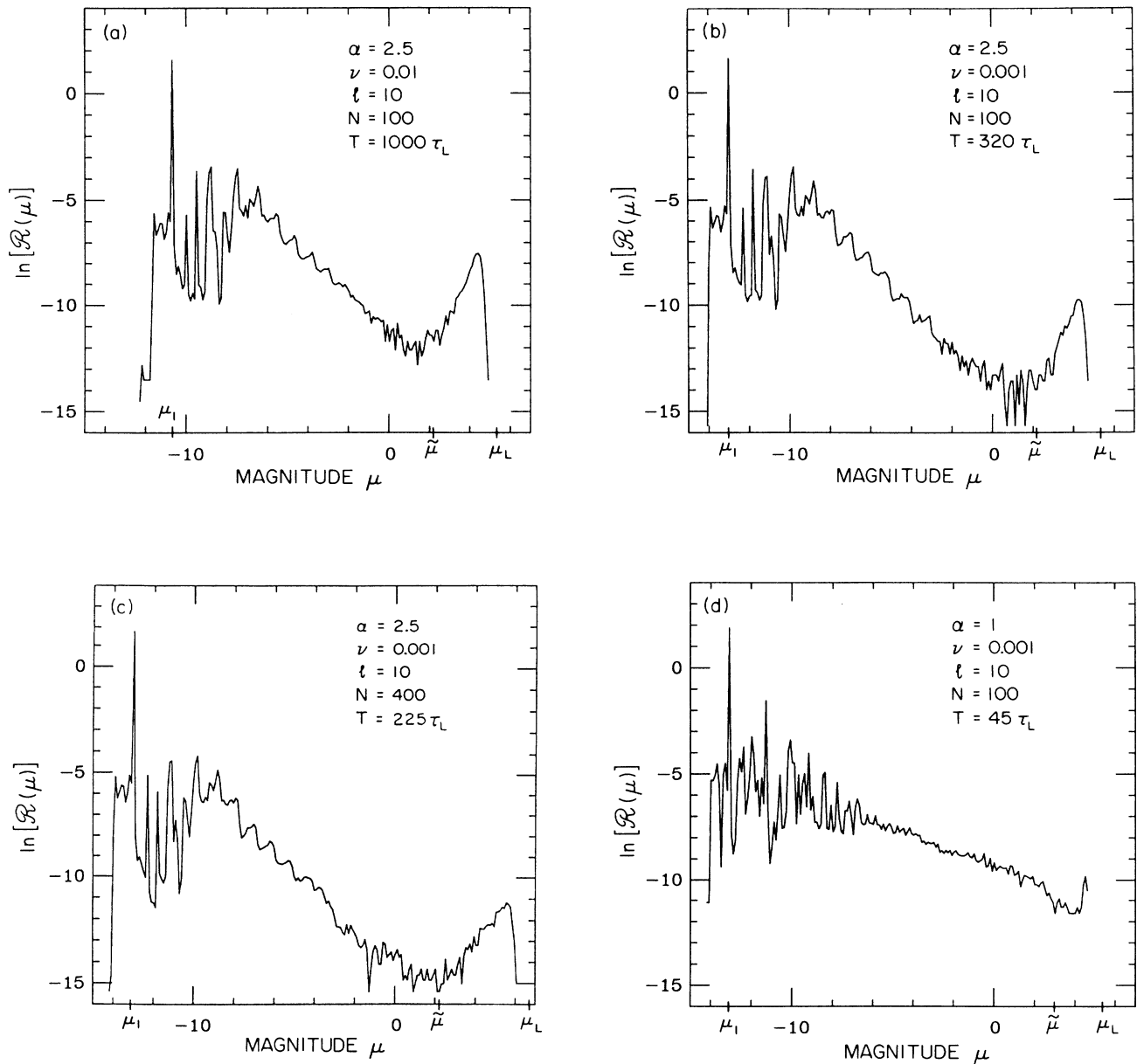


FIG. 6. Size distributions obtained from numerical simulations:  $\ln \mathcal{R}(\mu)$  as a function of  $\mu$  for various values of the system size  $N$ , the pulling speed  $\nu$ , and the parameters  $\alpha$  and  $l$ . For each graph, data were accumulated for the time  $T$ , given here in units of the loading time  $\tau_L = 2/\nu$ . The quantity  $\mu_1$  is the magnitude of one-block events given in Eq. (5.4);  $\bar{\mu} = \ln(2\xi/\alpha)$  is the magnitude of the largest localized event as predicted by (6.5); and  $\mu_L = \ln(2L)$  is the predicted magnitude of the largest event that the system can sustain.

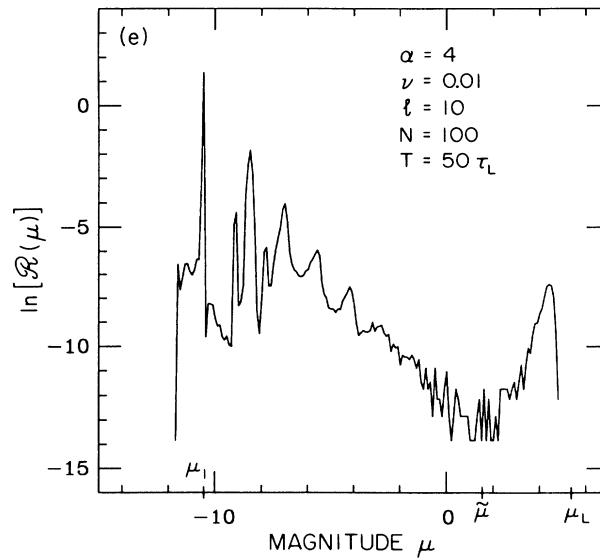


FIG. 6. (Continued).

value below which some qualitatively different kind of noisy but continuous creeping behavior occurs. On the other hand, it is also possible that this transition, if it happens at all, depends on the pulling speed  $\nu$ . In fact, we found it necessary to reduce  $\nu$  to 0.001 in Fig. 6(d) in order to obtain meaningful data. This point, which may be important for understanding the distinction between stability and instability in friction, clearly deserves further study.

## VI. SCALING THEORY

The structure of our version of the Burridge-Knopoff model is sufficiently simple that many aspects of the distributions shown in Fig. 6 can be understood by dimensional analysis combined with a liberal use of concepts that have become familiar in the theory of critical phenomena. We start by looking at  $\mathcal{R}_S(\mu)$  in the scaling region. Our earlier observation that position along the fault  $s = ja$  scales independently of the displacements of the blocks  $X_j = D_0 U_j$  now takes on special importance. In Eq. (2.8),  $U$  is a displacement (in units of  $D_0$ ),  $\nu$  has dimensions of displacement per unit time  $\tau$ , and the only quantity with the dimensions of length  $s$  is  $\xi$ . Of course, both the block spacing  $a$  and the size of the system  $L$  also are lengths that enter into the full statement of the problem. It seems plausible, however, to assume that the distribution of events in the scaling region is independent of either of the latter quantities, that is, that there is some range of sizes of events for which the continuum theory (2.8), by itself, is an adequate description.

The function  $\mathcal{R}_S(\mu)$  has dimensions of

$[(\text{length}) \times (\text{time})]^{-1}$ , and  $M$  has the dimensions of  $(\text{length}) \times (\text{displacement})$ ; thus a general form for  $\mathcal{R}_S$  under these assumptions is

$$\mathcal{R}_S(\mu) = \frac{\nu}{M} \mathcal{C} \left( \frac{\alpha M}{2\xi}, \alpha \right), \quad (6.1)$$

where  $\mathcal{C}$  is some function to be determined. The reason for choosing the dimensionless combination  $\alpha M / 2\xi$  as an argument for  $\mathcal{C}$  will become apparent in the next few paragraphs. In the scaling region,  $\mathcal{R}_S$  behaves like a power of  $M$ , and therefore we must be looking at the limit

$$\mathcal{C} \left( \frac{\alpha M}{2\xi}, \alpha \right) \approx \mathcal{C}_0(\alpha) \left( \frac{\alpha M}{2\xi} \right)^\eta, \quad \frac{\alpha M}{2\xi} \rightarrow 0. \quad (6.2)$$

Comparing (6.1) and (6.2) to (5.3), we see that  $b = 1 - \eta$  and  $A = \nu \mathcal{C}_0(\alpha / 2\xi)^\eta$ . In the language of critical exponents,  $-\eta$  is an "anomalous dimension." The Gutenberg-Richter law and most of our numerical results indicate that  $\eta$  is approximately zero, but we see departures from this law at small  $\alpha$  as shown in Fig. 6(d). Our current best estimates for  $b$  and  $\mathcal{C}_0$  are shown for various values of  $\alpha$  in Fig. 7.

The question that arises immediately is whether the limit in (6.2) is sensible. Are magnitudes of realistic earthquakes consistent with the condition  $M \ll 2\xi/\alpha$ ? Remember that  $\xi$  is the distance traveled by a sound signal during the slipping time for a great event of the kind shown in Fig. 3, and thus is of order kilometers for real faults. An earthquake in which a kilometer of the fault is displaced a distance of order unity (i.e.,  $D_0$  in dimensional units) is a truly colossal event. But that is only a part

of the story. The more interesting part is the physical—as opposed to purely dimensional—reason for using  $\alpha M/2\xi$  as the argument of the function  $\mathcal{C}$  in (6.3). The length  $2\xi/\alpha$  is a physically natural unit in which to measure moments of slipping events because it marks the transition between localized and delocalized events as described in the discussion following Eq. (4.17).

To see this, suppose that the stuck block at the edge of

a slipping zone has displacement  $U \cong 0$ ; that is, its pulling spring is neither stretched nor compressed. In order to dislodge this block, the adjacent slipping block must undergo a displacement of order  $\delta U \cong l^{-2}$ . (In terms of our original forces and spring constants, the latter condition is  $k_c \delta X \cong F_0 = k_p D_0$ .) Returning to (4.17), we have

$$\delta U(\Delta s) = \int d\tau \dot{u}(s_0 + \Delta s, \tau) \cong \frac{\nu a}{4l^2 \xi} \exp(\alpha \Delta s / \xi), \quad (6.3)$$

where  $\Delta s = s - s_0$  is the distance from the triggering pulse (somewhere near the center of the zone) to the position at which the displacement is being measured. Let  $\tilde{\xi}$  be twice that value of  $\Delta s$  in (6.5) such that the localization condition  $\delta U(\Delta s) \cong l^{-2}$  is just satisfied. That is,  $\tilde{\xi}$  is the full width of a slipping zone that is just marginally localized. Clearly,

$$\tilde{\xi} \approx \frac{2\xi}{\alpha} \ln \left[ \frac{4\xi}{\nu a} \right]. \quad (6.4)$$

The associated moment is

$$\tilde{M} = 2 \int_0^{\tilde{\xi}} \delta U(\Delta s) d(\Delta s) \approx 2\xi/\alpha. \quad (6.5)$$

Thus the natural argument for the function  $\mathcal{C}$  in (6.1) is  $M/\tilde{M} = \alpha M/2\xi$ . The magnitude  $\bar{\mu} = \ln \tilde{M}$  is indicated along the  $\mu$  axes in Fig. 6. As expected, this magnitude does mark the upper end of the scaling region.

In the language of critical phenomena,  $\tilde{\xi}$  is a correlation length; it is the characteristic size of the largest localized events. Note that it diverges logarithmically as  $\nu$  vanishes, implying that the pulling speed is the critical parameter in this theory. The scaling region comprises those events whose sizes  $\Delta s$  are in the range  $a \ll \Delta s \ll \tilde{\xi}$  or, equivalently, whose magnitudes  $\mu$  satisfy  $\mu_1 \ll \mu \ll \bar{\mu}$ . This is a critical region in the sense that all natural length scales have disappeared and thus the event within the scaling region must be self-similar.

Two further tests of the scaling assumption are shown in Fig. 6. According to (6.1), the function  $\mathcal{R}_S(\mu)/\nu$  should be independent of  $\nu$  in the scaling region. To check this, in Fig. 6(b), we have plotted  $\ln(\mathcal{R}_S)$  for  $\nu=0.001$  in order to compare it with the corresponding function in Fig. 6(a) for  $\nu=0.01$ . The agreement is excellent, the only difference being—as expected—that the vertical scales differ by a factor of  $\ln(10)$  and the microscopic events are shifted to smaller  $\mu$  for the smaller value of  $\nu$ . In this sense, the scaling region becomes larger as the critical parameter  $\nu$  approaches zero. Equation (6.1) also implies that  $\mathcal{R}_S(\mu)$  should be independent of  $L$  (for  $L$  sufficiently large). This is shown in Fig. 6(c), where we have increased the size of the system by a factor of 4 compared to Fig. 6(b), but have kept all other parameters the same. The only noticeable effect is that, as mentioned previously, the region of great events extends to larger  $\mu$  and the distribution  $\mathcal{R}_G(\mu)$  is less sharply peaked. Otherwise, the distributions are essentially identical in both the microscopic and scaling regions.

Let us turn now to the delocalized great events in the

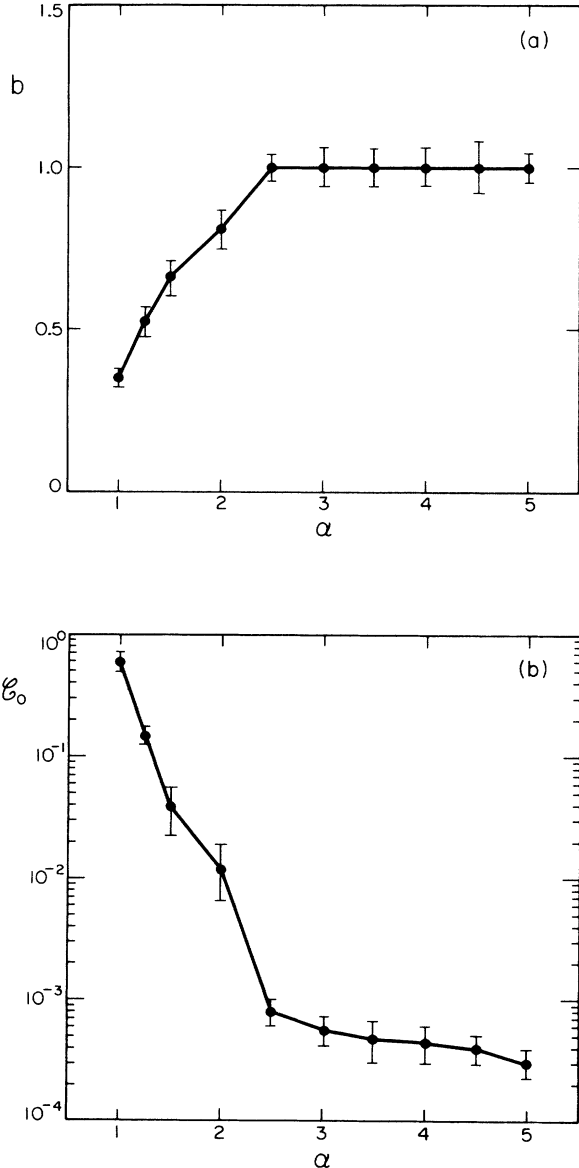


FIG. 7. The parameters  $b$  and  $\mathcal{C}_0$  which characterize the scaling distribution  $\mathcal{R}_S(\mu)$  as defined in Eq. (6.2). These results were obtained from the numerical calculations shown in Fig. 6 and other similar computations. All data shown here were obtained for  $l=10$ ,  $0.001 \leq \nu \leq 0.01$ , and  $100 \leq N \leq 400$ , and was accumulated for times  $T$  ranging between  $40\tau_L$  and  $1000\tau_L$ .

upper part of the distribution  $\mathcal{R}_G(\mu)$  where  $\mu > \bar{\mu}$ . An interesting quantity to consider is the integrated frequency of these events, i.e., the area under the distribution  $\mathcal{R}_G$ . To compute this, we use the identity

$$\int dM \mathcal{R}(\mu) = v. \quad (6.6)$$

This is simply a statement that the cumulative effect of all the events is to keep the blocks moving, on the average, at the pulling speed. Let  $\langle v \rangle_S$  denote the contribution to the left-hand side of (6.6) from events in the scaling and microscopic regions

$$\langle v \rangle_S = \int_{M_1}^{\bar{M}} dM \mathcal{R}_S(\mu), \quad (6.7)$$

where  $M_1 = \exp(\mu_1)$  is the moment of a one-block event as given in (5.4). Similarly, write

$$\langle v \rangle_G = \int_{\bar{M}}^{2L} dM \mathcal{R}_G(\mu) \equiv R_G M_G, \quad (6.8)$$

where

$$R_G = \int_{\bar{\mu}}^{\mu_L} d\mu \mathcal{R}_G(\mu) \quad (6.9)$$

is the integrated frequency of the great events per unit length of the fault, and  $M_G = \langle v \rangle_G / R_G$  is their average moment. Then, because

$$v = \langle v \rangle_S + \langle v \rangle_G, \quad (6.10)$$

the frequency of great events on the fault as a whole is

$$LR_G = \frac{Lv}{M_G} \left[ 1 - \frac{\langle v \rangle_S}{v} \right]. \quad (6.11)$$

In the case  $M_G \approx 2L$ , the first factor on the right-hand side of (6.11) is simply the loading frequency  $v/2$ . An obvious question is whether the localized events in the scaling region can move the system forward fast enough—that is, produce a large enough  $\langle v \rangle_S$ —to reduce significantly the frequency of great earthquakes.

To make further progress in answering questions of this kind, we must look at specific situations. According to Fig. 7,  $\eta \approx 0$  for  $\alpha \geq 2.5$ , in which case

$$\frac{\langle v \rangle_S}{v} \approx \mathcal{C}_0(\bar{\mu} - \mu_1). \quad (6.12)$$

Because  $\mu_1$  is proportional to  $\ln(v)$  according to (5.4), we could, in principle, pull the system slowly enough to make  $-\mu_1$  become large and thus make (6.12) approach unity. But, because  $\mathcal{C}_0 \approx 10^{-3}$ , “slowly enough” means  $v \approx 10^{-100}$  or less, which hardly seems reasonable. Our conclusion is that the great earthquakes in this regime of system parameters account for all but a few percent of the average motion of the fault.

For values of  $\alpha$  smaller than about 2.5, our simulations seem to indicate that  $\eta$  is positive. In this case, the microscopic events do not contribute at all to  $\langle v \rangle_S$ , and we can write

$$\frac{\langle v \rangle_S}{v} \approx \frac{\mathcal{C}_0}{\eta}. \quad (6.13)$$

For  $\alpha = 1.0$ , our estimates shown in Fig. 7 indicate that

the right-hand side of (6.13) is about unity and indeed the great events in this case, as seen in Fig. 6(d), are strongly suppressed.

## VII. QUESTIONS AND (A FEW) ANSWERS

A large number of questions are implied but left unanswered in the discussion so far. In the following paragraphs, we shall pose some of those questions explicitly and suggest a few answers.

(1) Is the Burridge-Knopoff model, as we have used it, at all realistic? The fractional contribution of localized events to the forward motion, i.e., the ratio  $\langle v \rangle_S / v$  in (6.10), seems to be much less than unity for all situations in which we find the Gutenberg-Richter law ( $b \approx 1$ ) to be valid. Does this result mean that the Burridge-Knopoff model is purely academic?

This is indeed worrisome. However, several points can be raised in defense of the model. In the first place, it is not known whether the actual distribution of magnitudes for a single real earthquake fault might not look qualitatively as predicted here, with a broad scaling region and excess events at large  $\mu$ . We do know that the very few great earthquakes that occur each year release more seismic energy than all the hundreds of thousands of smaller events combined, but the available statistical information is not good enough to establish with certainty whether the frequency of these events lies above the  $b \approx 1$  line.

Curiously, although the great events in our model (for large  $\alpha$ ) account for almost all the forward motion, it is the smaller events in which much of the frictional dissipation occurs. This is because most of the motion in the great events is at speeds so large that the force of friction is small. The net effect of a great event is that the potential energy of stretched pulling springs is converted into compression of these springs, and is hardly dissipated at all. The dissipative behavior of the system—in particular, the time-dependent relation between pulling speed and pulling force—is an interesting topic for further study.

Certainly, there are parameter ranges in our model for which the localized events in the scaling region would be very noticeable in the real world. The scaling region does not (necessarily) describe just a very slow, effectively stable creeping motion between periodic great events. Slipping zones for event well within the scaling region extend over appreciable fractions of the overall length of the fault. These events have magnitudes that are sufficiently close to  $\mu_L$  that they would lie well up on the Richter scale if we were to convert our logarithms to base ten and shift the  $\mu$  axis so that our great events occurred near, say, a magnitude of 8.

(2) What is the underlying length scale  $a$  for a real fault? Does it matter?

Although  $a$  does not appear explicitly in  $\mathcal{R}_S$  as given in (6.1), it does play an important role in the formula (6.4) for  $\bar{\xi}$  and also in the lower limit of the integration that defines  $\langle v \rangle_S$  in (6.7). The fact that  $a$  remains explicitly in these formulas for observable quantities is among the indications that our theory does not yet have a proper continuum limit. There is no *a priori* reason why there

should not be one or more fundamental small length scales in this model—for example, some characteristic size of crystallites, rocks, or segments of plates. It seems to us, however, that such an assumption would be unnecessarily ugly, and that a much simpler possibility exists.

Suppose that, instead of the idealized stick-slip friction law shown by the solid line in Fig. 2, we consider a modified law that admits stable viscous creep at speeds less than some very small  $v_0$ , as shown by the dashed line in that figure. Because the function  $\phi$  is now single valued everywhere, the continuum limit in (2.8) is well defined, and the one-block events that have played some role in our analysis must somehow be smoothed out.

To see how this happens, assume that the dimensionless pulling speed  $\nu$  is much greater than  $\nu_0 = v_0 / \omega_p D_0$ , and consider a portion of the fault that is creeping at a speed less than  $\nu_0$ , that is, a portion that would be considered stuck in our original formulation. A stability analysis like that summarized in Eqs. (3.2) and (3.3) tells us that small perturbations of wave number  $q$  decay at rates  $-\Omega(q)$ , where

$$\Omega(q) = -\alpha_0 \pm (\alpha_0^2 - 1 - \xi^2 q^2)^{1/2} \quad (7.1)$$

and  $\alpha_0 = 1/2\nu_0$  is very large and positive. We now ask the following: Which of these perturbations survive for an entire loading period and thus are effective in triggering new events, and which are damped out? The answer is that any perturbation for which  $q$  is sufficiently large that  $\Omega^+ > \nu/2$  is damped out, where  $\Omega^+$  denotes the slow mode (with the plus sign) in (7.1). The wave number at which this condition is marginally satisfied is

$$q_0 \cong \frac{1}{\xi} \left[ \frac{\nu}{2\nu_0} \right]^{1/2}. \quad (7.2)$$

Accordingly, the length  $a_0 = 1/q_0$  is the effective short-wavelength cutoff for this modified model; the continuum theory does not generate spatial structure on scales appreciably smaller than  $a_0$ . There is an interesting internal consistency to this choice of cutoff  $a = a_0$ . In this case, (7.2) becomes

$$\frac{\xi^2}{a^2} = l^2 = \frac{\nu}{2\nu_0}, \quad (7.3)$$

and then the average speed of one-block events in (4.9) is simply  $\delta W_1 / \delta \tau = \nu_0$ . Because  $\xi$  is known from the sound speed, Eq. (7.3) may provide a useful route for determining the remaining physical parameters in the theory.

(3) Are real faults long enough to be, so to speak, in the “thermodynamic limit?” What happens when they are not?

In the theory of thermodynamic critical phenomena, the intrinsic properties of a system are considered to be those that are obtained in a limit in which the size of the system is taken to infinity while all other parameters, including the critical parameters, are held fixed. For our system, the analogous limit would seem to require that  $\nu$  remain fixed while  $L/\xi$  becomes indefinitely large. If  $\xi$  itself is of order kilometers or more, and  $\xi$  diverges loga-

rithmically in  $\nu$  according to (6.4), then  $L/\xi$  for real earthquake faults is unlikely to be large enough to satisfy this limiting condition. In our numerical simulations,  $\xi/a \cong 66$  and 85 in Figs. 6(a) and 6(c), respectively; thus the limit is far from being achieved in Fig. 6(a) where  $L/a = 100$ , but may be reasonably well satisfied in Fig. 6(c) where  $L/a = 400$ .

For several reasons, however, the analogy to thermodynamic critical phenomena is not entirely accurate. The sum rule that determines the average speed, Eq. (6.10), must be satisfied under all circumstances, and this constraint on the spectrum of fluctuations has no parallel in the thermodynamic problem. So far as we can tell from the numerical experiments that have been completed at the time this paper is being written, the distribution of events in the scaling region is unaffected by the size of the system  $L$ , either in its functional form or its amplitude, so long as  $\nu$  is small enough. The only exception to this rule is that the scaling distribution may be truncated at some  $\mu < \bar{\mu}$  if  $L < \xi$ . For  $\alpha \geq 2.5$ , the overwhelmingly largest contribution to  $\nu$  in (6.10) comes from the delocalized great events, and all of these would have to lie in a peak near  $\mu = \mu_L = \ln(2L)$ , as in Fig. 6(a), if  $L$  is not sufficiently greater than  $\xi$ . When  $\alpha$  is small, this effect is less pronounced because the scaling distribution contributes appreciably to the sum rule (6.10), but a small value of  $L$  still ought to induce a peak at the upper end of the spectrum. In general, our analysis predicts that great earthquakes must recur almost periodically, once each loading time, on short faults.

We do not yet know what happens for very long faults. For large  $\alpha$ , the great events that account for the forward motion are distributed according to some  $\mathcal{R}_G(\mu)$  in the region  $\mu > \bar{\mu}$ , but we know little about this distribution. Presumably it is smooth. Because its integrated moment must be  $\langle \mu \rangle_G \cong \nu$ , and the upper limit for the integral that defines  $\langle \mu \rangle_G$  in (6.8) is now infinite, there must be a  $\nu$ -dependent upper cutoff in  $\mathcal{R}_G(\mu)$  or, equivalently, some characteristic magnitude of the great events. A similar statement can be made about the case of small  $\alpha$  except that, if the right-hand side of (6.13) is larger than unity, the  $\nu$ -dependent cutoff must lie in the scaling region. It remains to be seen, of course, whether real earthquake faults ever are long enough for these considerations to be relevant.

Finally, it should be noted that there is yet another physical length scale that, while completely irrelevant geologically, must be kept in mind in the interpretation of numerical simulations and possibly also in the design of laboratory experiments. This is the quantity  $2\xi/\nu$ , which is the distance traveled by a sound wave during a loading period. Ordinarily, this length should be much too large to play any role in the dynamics of real systems, but it can easily be chosen to be relatively small in simulations. We have found that, if we increase  $\nu$  to the point that  $2\xi/\nu$  becomes comparable to or smaller than  $L$ —that is, if the loading period becomes comparable to the time taken for a sound wave to traverse the fault—then we excite what appear to be resonant propagating modes, and our analysis in terms of isolated events breaks down. For example, this happened when we tried to use  $\nu = 0.01$ , with

$l=10$ , for systems as large as  $N=1000$ . Our tentative suggestion is that, for models of the kind considered here, the natural “thermodynamic limit” is one in which the critical parameter  $\nu$  vanishes as  $L$  becomes large in such a way that  $\xi \ll L \ll \xi/\nu$ .

(4) What important properties of real earthquake faults are missing in this model? What might their effects be?

The potentially most serious limitation of this model is its dimensionality. Real earthquake faults are two-dimensional interfaces between three-dimensional plates. Small slips occur in two-dimensional patches on this interface, but great earthquakes break the surface and propagate in a one-dimensional manner along the fault. In either case, the associated strain fields extend into the neighboring material in a way that cannot be modeled accurately by our coupling and pulling springs.

Dimensionality is extremely important in thermodynamic critical phenomena; it is one of a small number of relevant parameters that determine the “universality class” of a critical point. The model discussed here is so unconventional, however, that we do not know what the effective dimensionality is, or even whether the concept makes sense. It seems to us most likely that the two-dimensional nature of localized slipping events on the interface between two plates must change the scaling distribution significantly, but that the crossover between these events and the effectively one-dimensional propagating great events may correspond roughly to the delocalization transition in our theory. Clearly, more work needs to be done.

Another physically important feature that is missing in our model is the interaction between faults, or between remotely separated sections of a single fault. Because of the idealized stick-slip friction law that we have used, separated slipping zones cannot communicate with each other unless all the blocks in between them become unstuck. Not even sound waves propagate through a stuck region. As a result, we probably cannot expect to see aftershocks in this model; there is no way for one event to trigger another unless they are parts of the same slipping zone or are immediately adjacent to one another.

In the latter regard, it might be interesting to explore the effects of more realistic friction laws, perhaps with stable creep at small velocity as suggested in item (2) above, or with some combination of velocity hardening as well as weakening, or with nonzero friction at high speeds to simulate radiative losses. It is possible that many such effects will have to be considered in order to interpret aftershocks, swarms of events, quiescent periods and the like—that is, in order to understand the dynamic correlations that are important for predictive purposes. We have hardly touched upon such correlations in this paper, although they certainly do exist in this model.

They will have to be understood in terms of simple models such as this one before it will make sense to look at more complex situations.

## VIII. CONCLUSIONS

In summary, we note the following.

The spatially uniform Burridge-Knopoff model of an earthquake fault, with an idealized stick-slip friction law, generates deterministically a wide range of slipping events whose size distribution is similar in important respects to what is seen in nature. The persistently chaotic behavior of this model is a direct consequence of the friction law, which causes small irregularities in the system to be amplified during slipping motions.

The model produces three qualitatively distinct kinds of slipping events: microscopic events, involving motions on the smallest length scales accessible to the system; large but localized events; and delocalized, great events. The localized events are critical fluctuations; they are self-similar over a range of length scales which becomes infinitely broad in the limit of vanishing loading speed. The distribution in magnitudes of these localized events is consistent with the Gutenberg-Richter law.

In most of the cases studied here, the delocalized great events play the dominant role in moving the system forward on average at the loading speed. The degree to which this is true depends upon a single dimensionless group of parameters, denoted here by the symbol  $\alpha$ , which is the rate at which disturbances are amplified as a result of velocity-weakening friction. The length of the fault also plays a significant role in determining the relative frequency of great events. In general, great events are relatively more important and more nearly periodic on shorter faults and for larger values of  $\alpha$ .

Among the questions left unanswered in this paper is how the conclusions might be modified in a more realistic, three-dimensional model of an earthquake fault, or in a model with a more realistic friction law. Also, we have not discussed dynamic correlations between events in this model, nor have we addressed the problem of how to calculate the critical behavior from first principles.

## ACKNOWLEDGMENTS

We have benefited from useful discussions with J. Rice, R. Schumacher, C. Tang, H. Nakanishi, B. Shaw, and G. Swindle. This research was supported by U.S. Department of Energy Grant No. DE-FG03-84ER45108 and also in part by National Science Foundation Grant No. PHY82-17853, supplemented by funds from the National Aeronautics and Space Administration.

<sup>1</sup>P. Bak, C. Tang, and K. Wiesenfeld, *Phys. Rev. Lett.* **59**, 381 (1987); *Phys. Rev. A* **38**, 364 (1988); C. Tang and P. Bak, *Phys. Rev. Lett.* **60**, 2347 (1988); *J. Stat. Phys.* **51**, 7977 (1988).

<sup>2</sup>L. Kadanoff, S. Nagel, L. Wu, and S. Zhou, *Phys. Rev. A* **39**, 6524 (1989).

<sup>3</sup>The relevance of threshold fluctuations, i.e., “self-organized

criticality” to earthquake faults has been suggested by P. Bak and C. Tang (unpublished); (private communication). A related model has been studied by J. I. Katz, *J. Geophys. Res.* **91**, 10412 (1986).

<sup>4</sup>B. Gutenberg and C. F. Richter, *Ann. Geofis.* **9**, 1 (1956).

<sup>5</sup>R. Burridge and L. Knopoff, *Bull. Seismol. Soc. Am.* **57**, 341

- (1967).
- <sup>6</sup>Various versions of the Burridge-Knopoff block-and-spring model of an earthquake fault appear in the recent literature. For example, see J. Rundle and D. Jackson, *Bull. Seismol. Soc. Am.* **67**, 1363 (1977); A. Nur, *Pageoph.* **116**, 964 (1978); T. Cao and K. Aki, *ibid.* **122**, 10 (1984); H. Takayasu and M. Matsuzaki, *Phys. Lett. A* **131**, 244 (1988).
- <sup>7</sup>M. E. McIntyre, R. T. Schumacher, and J. Woodhouse, *Acustica* **49**, 13 (1981); *J. Acoust. Soc. Am.* **74**, 1325 (1983).
- <sup>8</sup>A short summary of these results is given in J. M. Carlson and J. S. Langer, *Phys. Rev. Lett.* **62**, 2632 (1989).
- <sup>9</sup>P. G. de Gennes, *Superconductivity of Metals and Alloys* (Benjamin, New York, 1966), pp. 82–91; P. W. Anderson, *Phys. Rev. Lett.* **9**, 309 (1962); P. W. Anderson and Y. B. Kim, *Rev. Mod. Phys.* **36**, 39 (1964).
- <sup>10</sup>S. N. Coppersmith and P. B. Littlewood, *Phys. Rev. B* **36**, 311 (1987).
- <sup>11</sup>S. Garoff (private communication).
- <sup>12</sup>J. H. Dieterich, *Pure Appl. Geophys.* **121**, 790 (1978).
- <sup>13</sup>A. L. Ruina, Ph.D. thesis, Brown University, 1980; *J. Geophys. Res.* **88**, 359 (1983).
- <sup>14</sup>J. R. Rice, *Pure Appl. Geophys.* **121**, 443 (1983).
- <sup>15</sup>J. R. Rice and A. L. Ruina, *J. Appl. Mech.* **50**, 343 (1983).
- <sup>16</sup>S. T. Tse and J. R. Rice, *J. Geophys. Res.* **91**, 9452 (1986).
- <sup>17</sup>F. Horowitz, Ph.D. thesis, Cornell University, 1989.